JST: Smart Systems and Devices
Volume 33, Issue 2, May 2023, 058-068

Adaptive Asymmetric Time-Varying Integral Barrier Lyapunov Control-Based Trajectory Tracking of Autonomous Vehicles

Nhu Toan Nguyen, Duc Thinh Le, Manh Cuong Nguyen, Danh Huy Nguyen, Tung Lam Nguyen*
Hanoi University of Science and Technology, Ha Noi, Vietnam
**Corresponding author email: lam.nguyentung@hust.edu.vn*

Abstract

The paper investigates the lane following and changing maneuvers of autonomous vehicles in the presence of unknown disturbances, taking into account the dynamic system states and input constraints. The integrated longitudinal-lateral and yaw rate dynamics of the vehicle are simultaneously considered to improve the tracking accuracy and system stability when navigating under critical conditions. Then, an adaptive asymmetric time-varying integral barrier Lyapunov control and dynamic surface control scheme are developed to design the active front steering controller, longitudinal controller, and direct yaw moment control controller, which is capable of constraining the system states and control signals within the predefined boundary. In addition, the radius basis function neural network (RBFNN) is employed to estimate the lumped disturbances caused by the parametric uncertainties, external disturbances, and unmodeled dynamics, and the command filter system is used to avoid the explosion of terms phenomenon. Due to the fast and accurate torque response characteristics of the in-wheel motors, the optimization-based method is then implemented to effectively allocate the driving/braking torque to each in-wheel motor so as to improve vehicle performance. The stability of the closed-loop system is comprehensively demonstrated by means of the Lyapunov theory. Finally, the quantitative and qualitative comparisons in different diving scenarios using the Carim-Simulink joint environment are carried out to illustrate the effectiveness and validation of the proposed method.

Keywords: Autonomous vehicle, asymmetric time-varying integral barrier, command filer system, radius basis function neural network, torque allocation, trajectory tracking.

1. Introduction

In recent years, the research on the development and application of the Advanced Driver Assistance System (ADAS) has been gaining increasing attraction in many countries, technology companies, and education institutes. ADAS is considered a breakthrough in the car automation industry because of its significant advantages, including lower energy consumption, the diminution of air pollution, and the improvement of passengers' comfort. Especially this system plays a crucial role in decreasing car accidents caused mostly by human errors, thus enhancing overall road safety [1]. ADAS, in general, composes a breadth of technologies such as lane departure warning, adaptive cruise control, automatic emergency braking, lane change assistance, traction control system, etc, which all incorporate to level up the driving experience [2]. Path tracking and stability handling are critical study aspects in ADAS involving improving vehicle safety and stability, which are primarily based on the longitudinal, lateral, and yaw dynamics of the vehicle.

In a majority of studies, the path tracking problem was generally approached as a problem of solely steering, neglecting other complexities of vehicle motion [3, 4]. Although the aforementioned works achieve important results, there exists a strong interdependence between the lateral and longitudinal motions of a vehicle, and the neglect of either one will adversely impact the vehicle's performance [5, 6]. Therefore, it is necessary to take into account both the longitudinal and lateral control simultaneously to enhance the control performance in a wide range of driving conditions. In [7], the integrated longitudinal and lateral dynamic model of the autonomous vehicle was presented for the high-speed lane-changing maneuver, and then the steering angle and traction/braking torque are calculated using the sliding mode control (SMC) method. In [8], the interval type-2 fuzzy sets control approach was developed for the integrated dynamic model, enabling the vehicle to robustly track the desired longitudinal speed and reference path simultaneously. Moreover, when navigating through adverse road conditions such as wet roads, or during critical maneuvers such as highspeed lane changes or high-curved roads, the tires will be slipped and express highly nonlinear characteristics, and the dynamic coupling effects be-tween the longitudinal and lateral motions will be intensified. In these cases, direct yaw moment control (DYC) is proven to be one of the most effective strategies to

ISSN: 2734-9373
https://doi.org/10.51316/jst.166.ssad.2023.33.2.8
Received: March 2, 2023; accepted: April 15, 2023

maintain vehicle stability and passenger comfort [9]. It is developed to exert the longitudinal force of each tire such that change the distribution of the driving/braking torque. In [10], the super-twisting sliding mode controller was developed for path-following maneuvers of the vehicle using the DYC and active front steering (AFS) integration systems, which enhances the accuracy and stability of the vehicle and eliminates the chattering phenomenon of the traditional SMC method. In [9], the integration model of DYC and AFS are controlled by the Takagi-Sugeno fuzzy control method considering the norm-bounded uncertainties of tire forces and time-varying longitudinal velocity to improve vehicle stability and achieve the H-infinity performance.

On the other hand, in practice, autonomous vehicles typically operate under a variety of constraints, stemming from the limitations of actuators such as steering, braking, and throttling systems, as well as the dynamic states of the vehicle, such as speed, acceleration, and yaw rate, in order to meet safety standards and ensure passenger comfort. However, in most previous works, these limitations are not taken into account. To deal with the constraints problem, the MPC method is typically considered a promising strategy. In [11], the authors presented an improved MPC strategy, which adaptively adjusted the weight of the cost function via the fuzzy system, and the magnitude of the steering angle and its rate are also constrained such that the tracking accuracy and driving comfort is enhanced. In [12], the MPC method was developed for lateral-longitudinal dynamic control problem, which takes into account the constraints of side slip angle and the control signals, hence improving the vehicle stability and control smoothness. However, with the increase in dynamic model complexity, system constraints, and prediction horizon, the MPC approach will significantly heighten the computational burden leading to an intractable problem or local optima solutions, despite the advantages in handling system constraints.

Inspired by the aforementioned works, this paper aims to address the issues of lane following and changing problems in autonomous vehicles by simultaneously considering the longitudinal-lateral control and DYC in presence of lumped disturbances. Furthermore, it is important to note that the constraints on the vehicle's states and actuators are also taken into account. The main contributions of this paper are summarized as follows.

(1) The system constraints problem of the autonomous vehicle is transformed into the state constraints control problem by extending the original system dynamic model. Then an asymmetric integral barrier Lyapunov function method is developed to ensure that the system states are all confined within predefined regions, thus the states and input signals of the original system always satisfy their respective constraints. In addition, the radial basis function neural network which is capable of approximating arbitrary nonlinear functions is employed to compensate for the lumped disturbances caused by the parametric uncertainties, external disturbances, and unmodeled dynamics, such that improving the accuracy and robustness of the system. In addition, the command filer system is utilized to estimate the derivative of virtual control signals, hence avoiding the "explosion of term" phenomenon.

(2) The comprehensive stability analysis of the closed-loop system is implemented to illustrate that all error signals are uniform ultimate boundedness (UUB) and that the constraints on the vehicle's states and actuators are always satisfied. The effectiveness of the proposed approach is illustrated by using the Carsim-Simulink joint environment in different driving scenarios and performance evaluation metrics.

2. Mathematical Model

In this study, a 7-DOF vehicle handling model of the autonomous car is taken into consideration as shown in Fig. 1, consisting of three motions on the yaw plane (x, y, and ψ) and four motions of vehicle wheels. The X-Y indicates the inertial coordinates, and the x-y is the vehicle body coordinates attached to the center of mass (COG). The mathematical dynamic model of the vehicle can be expressed as follows:

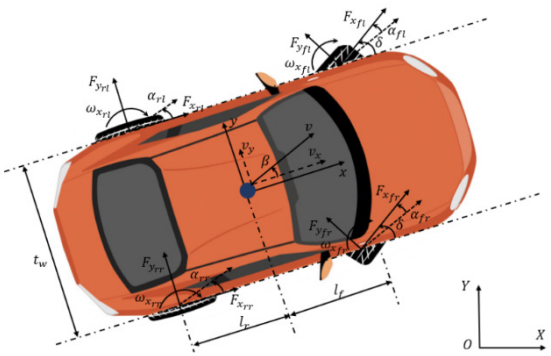

Fig. 1. 7-DOF vehicle handling model of the autonomous car

$$ma_x = (F_{x_{fl}} + F_{x_{fr}})\cos\delta - (F_{y_{fl}} + F_{y_{fr}})\sin\delta + (F_{x_{rl}} + F_{x_{rr}}) - F_{res} \quad (1)$$

$$ma_y = (F_{x_{fl}} + F_{x_{fr}})\sin\delta + (F_{y_{fl}} + F_{y_{fr}})\cos\delta + (F_{y_{rl}} + F_{y_{rr}}) \quad (2)$$

$$I_z\ddot{\psi} = l_f(F_{x_{fl}} + F_{x_{fr}})\sin\delta + l_f(F_{y_{fl}} + F_{y_{fr}})\cos\delta - l_r(F_{y_{rl}} + F_{y_{rr}}) + M_z \quad (3)$$

where m is the vehicle mass, I_z is the inertial moment around the yaw axis. l_f and l_r are distances from

the front and rear axles to the COG. $\ddot{\psi}$ denotes the angular acceleration of the vehicle around the yaw axis. F_x, F_y represent the longitudinal and lateral tyre forces respectively. The subscripts $(f,l),(f,r),(r,l)$, and (r,r) refer to the front-left, front-right, rear-left, rear-right tyres of the vehicle respectively. t_w is the distance from the left to the right tire. The direct yaw moment M_z considered as an additional control input to stabilize the vehicle motions are represented as:

$$M_z = l_f(F_{x_{fl}}+F_{x_{fr}})\sin\delta + 0.5t_w(-F_{x_{fl}} + F_{x_{fr}})\cos\delta + 0.5t_w(-F_{x_{rl}} + F_{x_{rr}}) \quad (4)$$

The longitudinal acceleration a_x and lateral acceleration a_y of the COG in the vehicle body coordinates are defined as:

$$\begin{aligned} a_x &= \dot{v}_x - v_y\dot{\psi} \\ a_y &= \dot{v}_y - v_x\dot{\psi} \end{aligned} \quad (5)$$

where A_F is the effective frontal area of the vehicle, ρ is the air density. C_d and C_{rr} are the aerodynamic drag coefficient an rolling friction coefficient respectively. The normal force on each wheel can be calculated as:

$$\begin{aligned} F_{z_{fl}} &= \left(k_{rx} - k_x\frac{a_x}{g}\right)\left(1-k_{fy}\frac{a_y}{g}\right),\ F_{z_{fr}} = \left(k_{rx} - k_x\frac{a_x}{g}\right)\left(1-k_{fy}\frac{a_y}{g}\right) \\ F_{z_{rl}} &= \left(k_{fx} - k_x\frac{a_x}{g}\right)\left(1-k_{ry}\frac{a_y}{g}\right),\ F_{z_{rr}} = \left(k_{fx} - k_x\frac{a_x}{g}\right)\left(1-k_{ry}\frac{a_y}{g}\right) \end{aligned} \quad (6)$$

with

$$k_{rx} = \frac{1}{2}mg\frac{l_r}{l}; k_{fx} = \frac{1}{2}mg\frac{l_f}{l}; k_x = \frac{1}{2}mg\frac{h}{l}; k_{ry} = \frac{h}{t_w}; k_{fy} = \frac{h}{t_w}$$

where h denotes the center of gravity height. The relationship between longitudinal forces and traction/braking torques is illustrated by the torque balance equation as:

$$I_w\dot{\omega}_{\tau,\epsilon} = -F_{x_{\tau,\epsilon}}r_w + \left(T_{d_{\tau,\epsilon}} - T_{b_{\tau,\epsilon}}\right) + \Delta T_{\tau,\epsilon} \quad (7)$$

with $\tau \in \{f,r\}, \epsilon \in \{l,r\}$. I_w is the moment of inertia of the wheel, ω indicates the wheel velocity, r_w is the effective wheel radius. T_d and T_b denote the total traction torque and the total braking torque executed on each wheel. $\Delta T_{\tau,\epsilon}$ represents the uncertainty of the model. To explicitly express the relationship between the driving/braking wheel torque and longitudinal velocity, (7) can be rewritten as:

$$\begin{aligned} F_{x_{\tau,\varepsilon}} &= \frac{1}{r_w}\left(T_{l_{\tau,\epsilon}} - I_w\dot{\omega}_{\tau,\epsilon}\right) + \frac{1}{r_w}\Delta T_{\tau,\epsilon} \\ &= \hat{F}_{x_{\tau,\varepsilon}} + \Delta F_{x_{\tau,\varepsilon}} \end{aligned} \quad (8)$$

where $T_{l_{\tau,\epsilon}} = T_{d_{\tau,\epsilon}} - T_{b_{\tau,\epsilon}}, \tau \in \{f,r\}, \epsilon \in \{l,r\}$. $\hat{F}_{x_{\tau,\varepsilon}}$ present the nominal longitudinal forces. Then, substituting (8) to (1) yields:

$$\begin{aligned} \dot{v}_x = &\frac{1}{m}\left[\frac{T_l}{r_w} - \frac{I_w\left(\dot{\omega}_{fl}+\dot{\omega}_{fr}\right)}{r_w}\cos\delta + \Delta F_{xf}\cos\delta\right] \\ &-\frac{1}{m}\left[\frac{I_w\left(\dot{\omega}_{rl}+\dot{\omega}_{rr}\right)}{r_w} + \Delta F_{xr} - F_{yf}\sin\delta - F_{res}\right] + v_y\dot{\psi} \end{aligned} \quad (9)$$

where $T_l = T_{l_{fl}}\cos\delta - T_{l_{fr}}\cos\delta + T_{l_{rl}} + T_{l_{rr}}$.

The longitudinal and lateral tire forces are expressed as follows [13]:

$$\begin{aligned} F_{x_{\tau,\varepsilon}} &= \left(\lambda_{x_{\tau,\varepsilon}}\cos\alpha_{\tau,\varepsilon} + \lambda_{y_{\tau,\varepsilon}}\sin\alpha_{\tau,\varepsilon}\right)\frac{\mu F_{z_{\tau,\varepsilon}}}{\sqrt{\lambda_{x_{\tau,\varepsilon}}^2 + \lambda_{y_{\tau,\varepsilon}}^2}} \\ F_{y_{\tau,\varepsilon}} &= \left(-\lambda_{x_{\tau,\varepsilon}}\sin\alpha_{\tau,\varepsilon} + \lambda_{y_{\tau,\varepsilon}}\cos\alpha_{\tau,\varepsilon}\right)\frac{\mu F_{z_{\tau,\varepsilon}}}{\sqrt{\lambda_{x_{\tau,\varepsilon}}^2 + \lambda_{y_{\tau,\varepsilon}}^2}} \end{aligned} \quad (10)$$

where $\lambda_{x_{\tau,\varepsilon}}, \lambda_{y_{\tau,\varepsilon}}$ are the slip ratio of each wheel in longitudinal and lateral directions, respectively, $\alpha_{\tau,\varepsilon}$ is slip angle of each tire. Assuming that the slip angle is small, (10) can be rewritten as:

$$\begin{aligned} F_{k_{\tau,\varepsilon}} &= \lambda_{y_{\tau,\varepsilon}}\frac{\mu F_{z_{\tau,\varepsilon}}}{\sqrt{\lambda_{x_{\tau,\varepsilon}}^2 + \lambda_{y_{\tau,\varepsilon}}^2}} + \Delta F_{k_{\tau,\varepsilon}} \\ &= \hat{F}_{k_{\tau,\varepsilon}} + \Delta F_{k_{\tau,\varepsilon}} \end{aligned} \quad (11)$$

where $k = \{x,y\}$, $\Delta F_{y_{\tau,\varepsilon}}$ accounts for the uncertainty of the model. The slip ratios can be approximated as:

$$\lambda_{x_{\tau,\varepsilon}} \approx \frac{\omega_{\tau,\varepsilon}r_w - v_{w_{\tau,\varepsilon}}}{\max\left\{\omega_{\tau,\varepsilon}r_w, v_{w_{\tau,\varepsilon}}\right\}} \quad (12)$$

$$\lambda_{y_{\tau,\varepsilon}} \approx \alpha_{\tau,\varepsilon} \quad (13)$$

with

$$\begin{aligned} v_{w_{fl}} &= V - \dot{\psi}\left(\frac{t_w}{2} - l_f\beta\right),\ v_{w_{fr}} = V + \dot{\psi}\left(\frac{t_w}{2} + l_f\beta\right) \\ v_{w_{rl}} &= V - \dot{\psi}\left(\frac{t_w}{2} + l_f\beta\right),\ v_{w_{rr}} = V + \dot{\psi}\left(\frac{t_w}{2} - l_f\beta\right) \\ \alpha_{fl} &= \delta - \arctan\left(\frac{v_y + l_f\dot{\psi}}{v_x}\right),\ \alpha_{fr} = \delta - \arctan\left(\frac{v_y + l_f\dot{\psi}}{v_x}\right) \\ \alpha_{rl} &= -\arctan\left(\frac{v_y - l_f\dot{\psi}}{v_x}\right),\ \alpha_{rr} = -\arctan\left(\frac{v_y - l_f\dot{\psi}}{v_x}\right) \end{aligned} \quad (14)$$

Substituting (13) to (2), the lateral dynamic can be written as:

$$\dot{v}_y = \frac{1}{m}\left(\left(F_{x_{fl}} + F_{x_{fr}}\right)\sin\delta + \left(F_{y_{rl}} + F_{y_{rr}}\right) - mv_x\dot{\psi}\right) - G_y \arctan\left(\frac{v_y + l_f\dot{\psi}}{v_x}\right) + G_y\delta \tag{15}$$

where

$$G_y = \left(\frac{\mu F_{z_{fl}}}{\sqrt{\lambda_{x_{fl}}^2 + \lambda_{y_{fl}}^2}} + \frac{\mu F_{z_{fr}}}{\sqrt{\lambda_{x_{fr}}^2 + \lambda_{y_{fr}}^2}}\right)\cos\delta$$

3. Problem Formulation

The control objectives are to follow the desired trajectory while maintaining vehicle stability during the maneuver. To closely follow the pre-defined trajectories, the steering angle is controlled to adjust the lateral force of the vehicle to minimize lateral deviation, while the longitudinal control is responsible for generating driving/braking torque to follow the speed profile. However, when the vehicle is in critical conditions, the lateral acceleration, yaw rate, and sideslip angle will be high, leading to the saturation phenomenon of tire lateral forces. In these cases, changing the steering angle only cannot improve the vehicle's yaw stability, so the DYC control is designed to apply the longitudinal force of each tire to change the distribution of driving/braking torque to improve the vehicle's yaw stability. In addition, since autonomous vehicles typically operate under a variety of constraints from dynamic states or actuator limitations, it is necessary to consider these constraints during the control design process. Therefore, this paper considers simultaneously longitudinal, lateral, and yaw motion of the vehicle to construct the tracking controllers which are capable of constraining vehicle states and control inputs.

3.1. Steering Control Formulation

For the purpose of precise tracking of the reference path, the steering control system is designed to regulate the steering angle in order to minimize the lateral deviation. The lateral tracking error is therefore defined as follows:

$$e_y = \int_o^t \left(v_x \sin\psi + v_y \cos\psi\right)dt - y_d \tag{16}$$

Let $\left(x_{1y}, x_{2y}\right)^T = \left(e_y, \dot{e}_y\right)^T$, the following system can be obtained:

$$\begin{aligned} \dot{x}_{1y} &= x_{2y} \\ \dot{x}_{2y} &= F_{ky} + G_{ky}\delta + D_y \end{aligned} \tag{17}$$

where

$$F_{ky} = \frac{1}{m}\left(\hat{F}_{xf}\sin\delta + \hat{F}_{yf}\right)\cos\psi - G_y \arctan\left(\frac{v_y + l_f\dot{\psi}}{v_x}\right)\cos\psi + v_x\dot{\psi}\cos\psi + \dot{v}_x\sin\psi - v_y\dot{\psi}\sin\psi - \ddot{y}$$

To enhance the lateral control performance, the steering controller is designed to ensure that the tracking error is always constrained by $e_y(t) \in \Omega_{y1} = \left\{e_y(t) \in \mathbb{R} \middle| k_{ny1}(t) < e_y(t) < k_{py1}(t)\right\}$. Assuming that the two desired tracking references are given as x_{1yd} and x_{yd}, respectively. The tracking error is defined as:

$$\begin{aligned} z_{1y} &= x_{1y} - x_{yd} \\ z_{2y} &= x_{2y} - \dot{x}_{yd} \end{aligned} \tag{18}$$

In addition, the AFS controller designed in this research directly controls the front steering wheel angles. Hence, to achieve a smooth transition, the magnitudes of the steering angle and its rate are constrained such that

$$\delta(t) \in \Omega_{y3} = \left\{\delta(t) \in \mathbb{R} \middle| k_{ny3}(t) < \delta(t) < k_{py3}(t)\right\},$$
$$\dot{\delta}(t) \in \Omega_{y4} = \left\{\dot{\delta}(t) \in \mathbb{R} \middle| k_{ny4}(t) < \dot{\delta}(t) < k_{py4}(t)\right\}.$$

To this end, the original lateral dynamic is expanded to include the second derivative of the steering angle, which allows for the transformation of the input constraint into a state constraint problem as follows:

$$\begin{aligned} \dot{x}_{1y} &= x_{2y} \\ \dot{x}_{2y} &= F_{ky} + G_{ky}\delta + D_y \\ \dot{\delta} &= \bar{\omega}_y \\ \dot{\bar{\omega}}_y &= U_y \end{aligned} \tag{19}$$

Then, the control signal U_y will be designed to stabilize this extended lateral system and guarantee the satisfaction of the constraints on e_y, δ, $\dot{\delta}$.

Assumption 1. Since $F_{x_{\tau,\varepsilon}}$ and $F_{y_{\tau,\varepsilon}}, \tau \in \{f, r\}$, $\varepsilon \in \{l, r\}$, are bounded due to limitations of the road surface adhesion and tire friction circle constraints, and the value of steering angle δ is relatively small in normal driving, hence it is feasible to assume that D_y is bounded by $\left|D_y\right| \le \lambda_y < \infty$.

3.2. Longitudinal and Direct Yaw Control Formulation

The longitudinal control generates the driving/braking torque T_l to pursue the desired speed, while the DYC induces the yaw moment M_z to stabilize the vehicle. Let $x_s = \left[v_x \;\; \dot{\psi}\right]^T$ and the tracking reference $x_{sd} = \left[v_{xd} \;\; \dot{\psi}_d\right]^T$, from (3) and (9), the following equation can be obtained:

$$\dot{x}_{sd} = F_{ks} + G_{ks}T_s + D_s \tag{20}$$

where

$$F_{ks} = \begin{bmatrix} F_{kx} & F_{k\gamma} \end{bmatrix}^T, G_{ks} = \begin{bmatrix} G_{kx} & G_{k\gamma} \end{bmatrix}^T, D_s = \begin{bmatrix} D_x & D_\gamma \end{bmatrix}^T$$

$$F_{kx} = -\big[\ I_w\left(\dot{\omega}_{fl} + \dot{\omega}_{fr}\right)\cos\delta + I_w\left(\dot{\omega}_{fl} + \dot{\omega}_{fr}\right) + r_w\hat{F}_{yf}\sin\delta / mr_w + v_y\dot{\psi}$$

$$F_{k\gamma} = 1/I_z\left[l_f\left(\hat{F}_{y_{fl}} + \hat{F}_{y_{fr}}\right)\cos\delta - l_f\left(\hat{F}_{y_{rl}} + \hat{F}_{y_{rr}}\right)\right]$$

$$G_{kx} = 1/\left(mr_w\right), G_{k\gamma} = 1/I_z, T_s = \begin{bmatrix} T_l & M_z \end{bmatrix}^T$$

$$D_x = \Big[\left(\Delta F_{x_{fl}} + \Delta F_{x_{fr}}\right)\cos\delta + \left(\Delta F_{x_{rl}} + \Delta F_{x_{rr}}\right) - \Delta F_{y_f}\sin\delta - F_{res}/m$$

$$D_x = 1/I_z\Big[l_f\left(\Delta F_{y_{fl}} + \Delta F_{y_{fr}}\right)\cos\delta - l_f\left(\Delta F_{y_{rl}} + \Delta F_{y_{rr}}\right) - 0.5t_w\left(-\Delta F_{y_{fl}} + \Delta F_{y_{fr}}\right)\sin\delta\ \Big]$$

In addition, for safety reasons, it is important to ensure that x_s is constrained by $x_s \in \Omega_{s1} = \left\{x_s(t) \in \mathbb{R}^2 \left| k_{ns1}(t) < x_s(t) < k_{ps1}(t) \right.\right\}$ $k_{ns1} = \begin{bmatrix} k_{nx1} & k_{n\gamma 1} \end{bmatrix}^T$, $k_{ps1} = \begin{bmatrix} k_{px1} & k_{p\gamma 1} \end{bmatrix}^T$. The tracking error $z_{1s} = \begin{bmatrix} z_{1x} & z_{1\gamma} \end{bmatrix}^T$ is considered as:

$$z_{1s} = x_s - x_{sd} \tag{21}$$

Besides, due to the limitations of actuators, the control torque T_l and yaw moment M_z are practically constrained such that

$$T_s \in \Omega_{s2} = \left\{T_s(t) \in \mathbb{R}^2 \left| k_{ns2}(t) < T_s(t) < k_{ps2}(t) \right.\right\},$$

$$k_{ns2} = \begin{bmatrix} k_{nx2} & k_{n\gamma 2} \end{bmatrix}^T,\ k_{ps2} = \begin{bmatrix} k_{px2} & k_{p\gamma 2} \end{bmatrix}^T.$$

For this purpose, the original dynamic system (20) is extended to the derivative of T_s to transform the input constraint into the state constraint problem as follows:

$$\begin{aligned} \dot{x}_s &= K_{ks} + G_{ks}T_s + D_s \\ \dot{T}_s &= U_s \end{aligned} \tag{22}$$

and the final control signal U_s is designed to ensure convergence of tracking error z_{1s} and the constraints of states v_x, $\dot{\psi}$, T_l, M_z of extended system (22).

Assumption 2. In reality, $F_{x_{\tau,\varepsilon}}$ and $F_{y_{\tau,\varepsilon}}, \tau \in \{f, r\}$, $\varepsilon \in \{l, r\}$, are bounded by restrictions of the road surface adhesion and tire friction circle constraints. Besides, the total resistance force is also bounded, and the value of steering angle δ is relatively small in normal driving, hence it is feasible to assume that D_s is bounded by $|D_s| \le \lambda_s < \infty$.

4. Controller Design

In this section, the design of the AFS, longitudinal control and DYC is achieved through the use of a proposed asymmetric integral barrier Lyapunov function control scheme, which takes into consideration the constraints of the dynamic states and control signals of the vehicle.

4.1. Active Front Steering Control

In order to drive the tracking error e_y towards zero, the following Lyapunov function is considered:

$$V_{1y} = \int_0^{z_{1y}} \frac{\sigma\left(k_{py1} - k_{ny1}\right)^2}{\left(y_d + \sigma - k_{ny1}\right)\left(k_{py1} - y_d - \sigma\right)} d\sigma \tag{23}$$

Taking the time derivative of V_{1y} yields:

$$\dot{V}_{1y} = \Xi_{11x}z_{1x}y_{2l} + \Xi_{12y}z_{1y}\dot{y}_d + \Xi_{13y}z_{1y}\dot{k}_{ny1} + \Xi_{14y}z_{1y}\dot{k}_{py1} \tag{24}$$

where $\Xi_{1iy}, i = \{1, 2, 3, 4\}$ are shown later in (49). Define the virtual control α_{1y} as:

$$\alpha_{1y} = -K_{1y}z_{1y} - K_{11yd}\Xi_{11y}z_{1y} - \Xi_{11y}^{-1}\left(\Xi_{12y}\dot{y}_d + \Xi_{13y}\dot{k}_{ny1} + \Xi_{14y}z_{1y}\dot{k}_{py1}\right) \tag{25}$$

where K_{1y}, K_{11yd} are positive designed parameters. To avoid repeating the calculation of the derivative which causes the problem of "explosion of complexity", the following command filtered system is designed:

$$\begin{aligned} \dot{\bar{\alpha}}_{1y} &= \varpi_{1y}\underline{\alpha}_{1y} \\ \dot{\underline{\alpha}}_{1y} &= -2\tau_{1y}\varpi_{1y}\underline{\alpha}_{1y} - \varpi_{1y}\left(\bar{\alpha}_{1y} - \Gamma\left(\underline{\alpha}_{1y}\right)\right) \end{aligned} \tag{26}$$

where α_{1y} and $\underline{\alpha}_{1y}$ are the outputs of the command filter satisfying $\alpha_{1y}(0) = 0$ and $\underline{\alpha}_{1y}(0) = 0$. $\varpi_{1y} > 0$ and $\tau_{1y} \in (0, 1]$ are the designed parameters. Let $z_{2y} = y_{2l} - \dot{\bar{\alpha}}_{1y}$ and $\epsilon_{1y} = \bar{\alpha}_{1y} - \alpha_{1y}$. Next, consider the following Lyapunov function:

$$V_{2y} = V_{1y} + \int_0^{z_{2y}} \left(\frac{\sigma\left(k_{py2} - k_{ny2}\right)^2}{\left(\bar{\alpha}_{1y} + \sigma + k_{ny2}\right)\left(k_{py1} - \bar{\alpha}_{1y} - \sigma\right)} \right) d\sigma + \frac{1}{2_{\gamma_y}}\tilde{W}_y^T\tilde{W}_y \tag{27}$$

Its derivative is:

$$\dot{V}_{2y} = \dot{V}_{1y} + \Xi_{21y}z_{2y}\left(F_{ky} + G_{ky}\delta + D_y\right) + \Xi_{22y}z_{2y}\dot{\bar{\alpha}}_{1y} + \Xi_{23y}z_{2y}\dot{k}_{ny2} + \Xi_{24y}z_{2y}\dot{k}_{py2} + \frac{1}{\gamma_y}\dot{\hat{W}}_y^T\tilde{W}_y \tag{28}$$

where Ξ_{2iy}, i = {1, 2, 3, 4} are shown in (49). Then, define the virtual control α_{2y} and the adaptive law $\dot{\hat{W}}_y$ as:

$$\alpha_{2y} = -\frac{1}{G_{ky}}\left(F_{ky} + \hat{W}_y^T\Theta_y\right) + \Xi_{21y}^{-1}\Xi_{11y}z_{1y} + K_{2y}z_{2y} + K_{21yd}\Xi_{21y}z_{2y} + K_{22yd}\Xi_{21y}G_{yk}^2 z_{2y} + \Xi_{21y}^{-1}\left(\Xi_{22y}\dot{\bar{\alpha}}_{1y} + \Xi_{23y}\dot{k}_{ny2} + \Xi_{24y}\dot{k}_{py2}\right) \tag{29}$$

$$\dot{\hat{W}}_y = \gamma_y\Xi_{21y}\Theta_y z_{2y} \tag{30}$$

where K_{2y}, K_{21yd}, $K_{22yd} > 0$. Passing α_{2y} through the command filtered system yields:

$$\begin{aligned}\dot{\bar{\alpha}}_{2y} &= \varpi_{2y}\underline{\alpha}_{2y}\\ \dot{\underline{\alpha}}_{2y} &= -2\tau_{2y}\varpi_{2y}\underline{\alpha}_{2y} - \varpi_{2y}\left(\bar{\alpha}_{2y} - \Gamma\left(\underline{\alpha}_{2y}\right)\right)\end{aligned} \tag{31}$$

where α_{2y} and $\underline{\alpha}_{2y}$ are the outputs of the command filter satisfying $\alpha_{2y}(0) = 0$, $\underline{\alpha}_{2y}(0) = 0$, $\varpi_{2y} > 0$ and $\tau_{2y} \in (0, 1]$. Let $z_{3y} = \delta - \bar{\alpha}_{2y}$ and $\epsilon_{2y} = \bar{\alpha}_{2y} - \alpha_{2y}$. Consider the following Lyapunov function:

$$V_{3y} = V_{2y} + \int_0^{z_{3y}}\left(\frac{\sigma\left(k_{py3} - k_{ny3}\right)^2}{\left(\bar{\alpha}_{2y} + \sigma + k_{ny3}\right)\left(k_{py13} - \bar{\alpha}_{2y} - \sigma\right)}\right)d\sigma \tag{32}$$

Its derivative is:

$$\dot{V}_{3y} = \dot{V}_{2y} + \Xi_{31y}z_{3y}\varpi_y + \Xi_{32y}z_{3y}\dot{\bar{\alpha}}_{2y} + \Xi_{33y}z_{3y}\dot{k}_{ny3} + \Xi_{34y}z_{3y}\dot{k}_{py3} \tag{33}$$

where Ξ_{3iy}, $i = \{1, 2, 3, 4\}$ are shown later in (49). Then, the virtual control signal ϖ_y is designed as:

$$\alpha_{3y} = -K_{3y}z_{3y} - K_{31yd}\Xi_{31y}z_{3y} - \Xi_{31y}^{-1}\Xi_{21y}z_{2y} - \Xi_{31y}^{-1}\left(\Xi_{32y}\dot{\bar{\alpha}}_{2y} + \Xi_{33y}\dot{k}_{ny3} + \Xi_{34y}\dot{k}_{py3}\right) \tag{34}$$

where K_{3y}, $K_{31yd} > 0$. Passing α_{3y} through command filtered system designed as:

$$\begin{aligned}\dot{\bar{\alpha}}_{3y} &= \varpi_{3y}\underline{\alpha}_{3y}\\ \dot{\underline{\alpha}}_{3y} &= -2\tau_{3y}\varpi_{3y}\underline{\alpha}_{3y} - \varpi_{3y}\left(\bar{\alpha}_{3y} - \Gamma\left(\underline{\alpha}_{3y}\right)\right)\end{aligned} \tag{35}$$

where α_{3y} and $\underline{\alpha}_{3y}$ are the outputs of the command filter satisfying $\alpha_{3y}(0) = 0$, $\underline{\alpha}_{3y}(0) = 0$, $\varpi_{3y} > 0$ and $\tau_{3y} \in (0,1]$. Let $z_{4y} = \varpi - \bar{\alpha}_{3y}$ and $\epsilon_{3y} = \bar{\alpha}_{3y} - \alpha_{3y}$. Consider the following Lyapunov function:

$$V_{4y} = V_{3y}\int_0^{z_{4y}}\left(\frac{\sigma\left(k_{py4} - k_{ny4}\right)^2}{\left(\bar{\alpha}_{3y} + \sigma + k_{ny4}\right)\left(k_{py14} - \bar{\alpha}_{3y} - \sigma\right)}\right)d\sigma \tag{36}$$

Its derivative is:

$$\dot{V}_{4y} = \dot{V}_{3y} + \Xi_{41y}z_{4y}\varpi_y + \Xi_{42y}z_{4y}\dot{\bar{\alpha}}_{3y} + \Xi_{43y}z_{4y}\dot{k}_{ny4} + \Xi_{44y}z_{4y}\dot{k}_{py4} \tag{37}$$

where Ξ_{4iy}, $i = \{1, 2, 3, 4\}$ are shown later in (49). From that, the final control signal U_y is designed as:

$$U_y = -K_{4y}z_{4z} - \Xi_{41y}^{-1}\Xi_{31y}z_{3y} - \Xi_{41y}^{-1}\left(\Xi_{42y}\dot{\bar{\alpha}}_{2y} + \Xi_{43y}\dot{k}_{ny4} + \Xi_{44y}\dot{k}_{py4}\right) \tag{38}$$

where $K_{4y} > 0$.

4.2. Longitudinal Control and DYC

Consider the following Lyapunov function:

$$V_{1s} = \int_0^{z_{1x}}\left(\frac{\sigma\left(k_{px1} - k_{nx1}\right)^2}{\left(\nu_{xd} + \sigma + k_{nx1}\right)\left(k_{px1} - \nu_{xd} - \sigma\right)}\right)d\sigma + \int_0^{z_{1\gamma}}\left(\frac{\sigma\left(k_{p\gamma 2} - k_{n\gamma 1}\right)^2}{\left(\dot{\psi}_d + \sigma - k_{n\gamma 1}\right)\left(k_{p\gamma 1} - \dot{\psi}_d - \sigma\right)}\right)d\sigma + \tilde{W}_s^T\Upsilon_s\tilde{W}_s \tag{39}$$

Its derivative is:

$$\dot{V}_{1s} = z_{1s}^T\Xi_{11s}\left(F_{ks} + G_{ks}M_s + D_s\right) + z_{1s}^T\Xi_{12s}\dot{x}_{sd} + z_{1s}^T\Xi_{13s}\dot{k}_{ns1} + z_{1s}^T\Xi_{14s}\dot{k}_{ps1} + \dot{\hat{W}}_s^T\Upsilon_s^{-1}\tilde{W}_s \tag{40}$$

Define the virtual control $\alpha_{1s} = \left[\alpha_{1x}\ \alpha_{1\gamma}\right]^T$ and the adaptive law $\dot{W}_s$ as:

$$\alpha_{1s} = -G_{ks}^{-1}\left(F_{ks} + \hat{W}_s\Theta_s + \Xi_{11s}^{-1}\left(\Xi_{12s}\dot{x}_{sd} + \Xi_{13s}\dot{k}_{ns1} + \Xi_{14s}\dot{k}_{ps1}\right) + K_{1s}z_{1s} + K_{11sd}\Xi_{11s}^T z_{1s} + K_{12sd}G_{ks}G_{ks}^T\Xi_{11s}^T z_{1s}\right) \tag{41}$$

$$\dot{W}_s = \Upsilon_s^T\Theta_s^T z_{1s} \tag{42}$$

where $K_{1s} = \mathrm{diag}(K_{1x}, K_{1\gamma})$, $K_{11sd} = \mathrm{diag}(K_{11xd}, K_{11\gamma d})$, $K_{12sd} = \mathrm{diag}(K_{12xd}, K_{12\gamma d})$ are positive designed parameters. Passing α_{1s} through command filtered system yields:

$$\begin{aligned}\dot{\bar{\alpha}}_{1s} &= \varpi_{1s}\underline{\alpha}_{1s}\\ \dot{\underline{\alpha}}_{1s} &= -2\tau_{1s}\varpi_{1s}\underline{\alpha}_{1s} - \varpi_{1s}\left(\bar{\alpha}_{1s} - \Gamma\left(\underline{\alpha}_{1s}\right)\right)\end{aligned} \tag{43}$$

where $\bar{\alpha}_{1s}$ and $\underline{\alpha}_{1s}$ are the outputs of the command filter satisfying $\bar{\alpha}_{1s}(0) = 0$ and $\underline{\alpha}_{1s}(0) = 0$. $\varpi_{1s} > 0$ and $\tau_{1s} \in (0, 1] \times (0, 1]$ are the designed parameters. Let $z_{2s} = \left[z_{2x}\ z_{2\gamma}\right]^T = T_s - \bar{\alpha}_{1s}$ and $\epsilon_{1s} = \bar{\alpha}_{1s} - \alpha_{1s}$. Next, consider the following Lyapunov function:

$$V_{2s} = \int_0^{z_{2x}}\left(\frac{\sigma\left(k_{px2} - k_{nx2}\right)^2}{\left(\bar{\alpha}_{1x} + \sigma - k_{nx2}\right)\left(k_{px2} - \bar{\alpha}_{1x} - \sigma\right)}\right)d\sigma + \int_0^{z_{2\gamma}}\left(\frac{\sigma\left(k_{p\gamma 2} - k_{n\gamma 2}\right)^2}{\left(\bar{\alpha}_{1\gamma} + \sigma - k_{n\gamma 2}\right)\left(k_{p\gamma 2} - \bar{\alpha}_{1\gamma} - \sigma\right)}\right)d\sigma \tag{44}$$

Taking the time derivative of V_{2s} yields:

$$\dot{V}_{2s} = \dot{V}_{1s} + z_{2s}^T\Xi_{12s}U_s + z_{2s}^T\Xi_{22s}\dot{\bar{\alpha}}_{1s} + z_{2s}^T\Xi_{23s}\dot{k}_{ns2} + z_{2s}^T\Xi_{24s}\dot{k}_{ps2} \tag{45}$$

The control law Us is designed as:

$$U_s = -K_{2s}z_{2s} - \Xi_{21s}^{-1}G_{ks}^T\Xi_{11y}^T z_{1s} + \Xi_{21s}^{-1}\left(\Xi_{22s}\dot{\bar{\alpha}}_{1s} + \Xi_{23s}\dot{k}_{ns2} + \Xi_{24s}\dot{k}_{ps2}\right) \tag{46}$$

where $K_{2s} = \text{diag}(K_{2x}, K_{2\gamma}) > 0$.

4.3. Stability Analysis

Assumption 3. The initial values of the autonomous vehicle' states $\chi=\{x_{1y}, x_{2y}, \nu_x, \dot{\psi}, \delta, \dot{\delta}, T_l, M_z\}$ satisfy $\chi(0) \in \Omega_a = \Omega_{y1} \times \Omega_{y2} \times \Omega_{s1} \times \Omega_{y3} \times \Omega_{y4} \times \Omega_{s2}$.

Lemma 1. Consider the following type of asymmetric integral barrier Lyapunov function:

$$V\left(z,a,k_n(t),k_p(t)\right)=\int_0^z\left(\frac{\sigma\left(k_p(t)-k_n(t)\right)^2}{\left(\alpha+\sigma-k_n(t)\right)\left(k_p(t)-\alpha-\sigma\right)}\right)d\sigma$$
$$=\left(k_p(t)-k_n(t)\right)\left(\left(\alpha-k_n(t)\right)\ln\frac{k_n(t)+\alpha}{k_n(t)+z+\alpha}\right.$$
$$\left.+\left(k_p(t)-\alpha\right)\ln\frac{k_p(t)-\alpha}{k_p(t)-z-\alpha}\right) \tag{47}$$

where $z=x-\alpha$ is the tracking error, α is the desired tracking trajectory, $k_n(t), k_p(t)$ are the time-varying constraint function. The following inequalities are hold in the set $\Omega=\left\{x\in R \mid k_n(t)<x<k_p(t)\right\}$:

$$\frac{z^2}{2}\le V\left(z,\alpha,k_n(t),k_p(t)\right)\le\frac{z^2\left(k_p(t)-k_n(t)\right)^2}{\left(z+\alpha-k_n(t)\right)\left(k_p(t)-z-\alpha\right)} \tag{48}$$

Proof of Lemma 1.

The expressions of Ξ_{ijy}, Ξ_{ijs}, $i = \{1, 2, 3, 4\}, j = \{1, 2, 3, 4\}$, $\alpha_{iy}=\left\{x_{yd},\bar{\alpha}_{1y},\bar{\alpha}_{2y},\bar{\alpha}_{3y}\right\}$, $\alpha_{ix}=\left\{\nu_{xd},\bar{\alpha}_{1x}\right\}, l=\{x,y,\gamma\}$ in (24), (28), (33), (37), (40), and (45) are given as:

$$\Xi_{i1s}=\left[\Xi_{i1s}\ \ \Xi_{i1\gamma}\right]^T,\ \ \Xi_{i2s}=\left[\Xi_{i2s}\ \ \Xi_{i2\gamma}\right]^T$$
$$\Xi_{i3s}=\left[\Xi_{i3s}\ \ \Xi_{i3\gamma}\right]^T,\ \ \Xi_{i4s}=\left[\Xi_{i4s}\ \ \Xi_{i4\gamma}\right]^T$$
$$\Xi_{i1s}=-\frac{\left(k_{pli}-k_{nli}\right)^2}{\left(k_{nli}-\alpha_{il}-z_{is}\right)\left(k_{pli}-\alpha_{il}-z_{is}\right)}$$
$$\Xi_{i2s}=\frac{k_{pli}-k_{nli}}{z_{il}}\ln\frac{\left(k_{nli}-\alpha_{il}\right)\left(k_{pli}-\alpha_{il}-z_{il}\right)}{\left(k_{pli}-\alpha_{il}\right)\left(k_{nli}-\alpha_{il}-z_{il}\right)}$$
$$\Xi_{i3s}=\frac{k_{pli}-k_{nli}}{z_{il}}\left(\ln\frac{k_{nli}-\alpha_{il}}{k_{nli}-\alpha_{il}-z_{il}}-\frac{z_{il}}{k_{nli}-\alpha_{il}-z_{il}}\right)$$
$$-\frac{k_{nli}-\alpha_{il}}{z_{il}}\ln\frac{k_{nli}-\alpha_{il}}{k_{nli}-\alpha_{il}-z_{il}}+\frac{k_{pli}-\alpha_{il}}{z_{il}}\ln\frac{k_{nli}-\alpha_{il}}{k_{nli}-\alpha_{il}-z_{il}}$$
$$\Xi_{i4s}=\frac{k_{nli}+k_{pli}}{z_{il}}\left(\ln\frac{k_{pli}-\alpha_{il}}{k_{pli}-\alpha_{il}-z_{il}}+\frac{z_{il}}{k_{pli}-\alpha_{il}-z_{il}}\right)$$
$$+\frac{k_{nli}+\alpha_{il}}{z_{il}}\ln\frac{k_{nli}+\alpha_{il}}{k_{nli}+\alpha_{il}+z_{il}}+\frac{k_{pli}-\alpha_{il}}{z_{il}}\ln\frac{k_{pli}-\alpha_{il}}{k_{pli}-\alpha_{il}-z_{il}} \tag{49}$$

Let $f\left(z,\alpha,k_n,k_p\right)=V\left(z,\alpha,k_n,k_p\right)-\frac{z^2}{2}$, Taking the partial time derivative of f with respect to z yields:

$$\frac{\partial f}{\partial z}=-z\frac{\left(k_p-k_n\right)^2+\left(k_n-x\right)^2+\left(k_p-x\right)^2}{2\left(k_n-x\right)\left(k_p-x\right)}$$

One can be seen that

$$\forall x\in\Omega=\left\{x\in R \mid k_n(t)<x<k_p(t)\right\},\qquad \partial f/\partial x=0$$

when $z=0$, $\partial f/\partial x>0$ when $z>0$, $\partial f/\partial x<0$, when $z<0$.

It means that $f\left(z,\alpha,k_n,k_p\right)\ge f\left(0,\alpha,k_n,k_p\right)=0$.

Hence $V\left(z,\alpha,k_n,k_p\right)\ge\frac{z^2}{2}$.

Define

$$g\left(\alpha,\sigma,k_n,k_p\right)=\frac{\sigma\left(k_p(t)-k_n(t)\right)^2}{\left(\alpha+\sigma-k_n(t)\right)\left(k_p(t)-\alpha-\sigma\right)}.$$

Taking the partial time derivative of g with respect to σ yields:

$$\frac{\partial g}{\partial\sigma}=-\frac{\left(k_p-k_n\right)^2\left(\sigma^2-\left(k_n-\alpha\right)\left(k_p-\alpha\right)\right)}{\left(k_n-\sigma-\alpha\right)^2\left(k_p-\sigma-\alpha\right)^2}>0$$

Therefore, $\int_0^z g\left(\alpha,\sigma,k_n,k_p\right)d\sigma=zg\left(\alpha,z,k_n,k_p\right)$,

which means that:

$$V\left(z,\alpha,k_n(t),k_p(t)\right)\le\frac{z^2\left(k_p(t)-k_n(t)\right)^2}{\left(z+\alpha-k_n(t)\right)\left(k_p(t)-z-\alpha\right)}$$

It completes the proof.

Theorem 1. Considering the closed-loop system of the 7-DOF autonomous vehicle (19) and (22). With the control signals (38), (46), filtering systems (26), (31), (35), (43), adaptive laws (30), (42), Assumption 1, and appropriately designed parameters, all the signals of the closed-loop system are PFS, and furthermore the system's states χ are always constrained by Ω_a.

Proof of Theorem 1.

The complete Lyapunov function of the system is given by:

$$V_a=V_{4y}+V_{2s} \tag{C.1}$$

Taking its time derivative and using the results of (25), (29), (34), (38), (41) and (46), we obtain:

$$\begin{aligned}\dot{V}_a &= \dot{V}_{4y} + \dot{V}_{2s} \\ &= -K_{1y}\Xi_{1y}z_{1y}^2 - K_{11yd}\Xi_{1y}^2 z_{1y}^2 - K_{2y}\Xi_{21y}z_{2y}^2 - K_{21yd}\Xi_{21y}^2 z_{2y}^2 \\ &\quad - K_{22yd}\Xi_{21y}^2 G_{yk}^2 z_{2y}^2 - K_{3y}\Xi_{31y}z_{3y}^2 - K_{31yd}\Xi_{31y}^2 z_{2y}^2 - K_{41yd}\Xi_{41y}z_{4y}^2 \\ &\quad - z_{1s}^T\Xi_{11s}K_{1s}z_{1s} - z_{1s}^T\Xi_{11s}K_{11sd}\Xi_{11s}^T z_{1s} \\ &\quad - z_{1s}^T\Xi_{11s}G_{ks}K_{12sd}G_{ks}^T\Xi_{11s}^T z_{1s} - z_{2s}^T\Xi_{21s}K_{2s}z_{2s} + \Xi_{3y}z_{3y}\epsilon_{3y} \\ &\quad + z_{1s}^T\Xi_{11s}\left(\eta_s + G_{ks}\,\epsilon_{1s}\right) + \Xi_{1y}z_{1y}\epsilon_{1y} + \Xi_{2y}z_{2y}\left(G_{ky}\epsilon_{2y} + \eta_y\right)\end{aligned}$$

By making use of Young's inequality, we obtain:

$$\Xi_{11y}z_{1y}\epsilon_{1y} \le K_{11yd}\Xi_{11y}^2 z_{1y}^2 + \frac{1}{4K_{11yd}}\epsilon_{1y}^2$$

$$\Xi_{21y}z_{2y}\eta_y \le K_{21yd}\Xi_{2y}^2 z_{2y}^2 + \frac{1}{4K_{21yd}}\eta_y^2$$

$$\Xi_{21y}z_{2y}G_{yk}\epsilon_{2y} \le K_{22yd}\Xi_{2y}^2 G_{yk}^2 z_{2y}^2 + \frac{1}{4K_{22yd}}\epsilon_y^2$$

$$\Xi_{31y}z_{3y}\epsilon_{3y} \le K_{31yd}\Xi_{31y}^2 z_{3y}^2 + \frac{1}{4K_{31yd}}\epsilon_{3y}^2$$

$$z_{1s}\Xi_{11s}^T\eta_s \le z_{1s}^T\Xi_{11s}K_{11sd}\Xi_{11s}^T z_{1s} + \frac{1}{4}\eta_s^T K_{11sd}^{-1}\eta_s$$

$$z_{1s}\Xi_{11s}^T G_{ks}\epsilon_{1s} \le z_{1s}^T\Xi_{11s}G_{ks}K_{12sd}G_{ks}^T\Xi_{11s}^T z_{1s} + \frac{1}{4}\epsilon_{1s}^T K_{11sd}^{-1}\epsilon_{1s}$$

Then $\dot{V}_a$ becomes:

$$\begin{aligned}\dot{V}_a &\le -K_{1y}\Xi_{11y}z_{1y}^2 - K_{2y}\Xi_{21y}z_{2y}^2 - K_{3y}\Xi_{31y}z_{3y}^2 - K_{4y}\Xi_{41y}z_{4y}^2 \\ &\quad - z_{1s}^T\Xi_{11s}K_{1s}z_{1s} - z_{2s}^T\Xi_{21s}K_{21s}z_{2s} + \epsilon_{1y}^2/\left(4K_{11yd}\right) + \epsilon_{2y}^2/\left(4K_{22yd}\right) \\ &\quad + \eta_y^2/\left(4K_{21yd}\right) + \epsilon_{3y}^2/\left(4K_{31yd}\right) + 4\eta_s^T K_{11sd}^{-1}\eta_s + 4\epsilon_s^T K_{12sd}^{-1}\epsilon_s \\ &\le -\sum_{i=1}^{4} K_{iy}V_{iy} - \sum_{i=1}^{2}\min\left\{K_{ix}, K_{i\gamma}\right\}V_{is} + \Delta_a \\ &\le -k_a V_a + \Delta_a\end{aligned}$$

where $k_a = \min\{K_{1x}, K_{2x}, K_{1y}, K_{2y}, K_{3y}, K_{4y}, K_{1\gamma}, K_{2\gamma}\}$,

$$\Delta_a = 1/2\sum\nolimits_{j=\{x,y,\gamma\}}\tilde{W}_j^T\tilde{W}_j + \epsilon_{1y}^2/\left(4K_{11yd}\right) + \epsilon_{2y}^2/\left(4K_{22yd}\right)$$

$$+\eta_y^2/\left(4K_{21yd}\right) + \epsilon_{3y}^2/\left(4K_{31yd}\right) + 4\eta_y^T K_{11sd}^{-1}\eta_s + 4\epsilon_y^T K_{12sd}^{-1}\epsilon_s$$

It completes the proof.

5. Evaluation by Co-Simulation

In this section, the performance of the proposed approach is verified by using the Carsim-Matlab joint environment. Many automotive manufacturers and design companies (such as Toyota, Mitsubishi, Delphi, and General Motors, to name a few) use CarSim in both model-in-the-loop and hardware-in-the- loop tests [14] as it can provide comprehensive full-car dynamic model and simulates the sophisticated behavior of the vehicle with high fidelity. While the vehicle dynamics are performed by CarSim simulation software, Matlab/Simulink is employed to embed the controller.

5.1. Simulation Setting

The vehicle drives on the dry road (μ = 0.9) and executes the double lane change maneuver (DLC) while undergoing the changes in longitudinal velocity. It starts from 22.3 m/s then increases to 25.8 m/s before decreasing to 18.5 m/s so that the DLC is performed during both acceleration and deceleration cases. The comparisons are carried out between a conventional SMC control scheme that evenly distributes the driving/braking torque without using DYC, the proposed control method, and an SMC control scheme that uses DYC and optimized-based torque distribution (SMC+DYC) to evaluate their respective performance. To ensure a smooth transition and to respect the physical limitations of the actuators, the constraints for steering angle δ, steering rate $\dot{\delta}$, driving torque T_l, external yaw moment Mz are defined as $-12^o \le \delta \le 12^o$, $-25^o \cdot s{-}1 \le \dot{\delta} \le 25^o \cdot s^{-1}$, $-1000\text{N}\cdot\text{m} \le T_l \le 1000\text{N}\cdot\text{m}$, $-4000\text{N}\cdot\text{m} \le M_z \le 4000\text{N}\cdot\text{m}$. In terms of system constraints, the vehicle's longitudinal speed is limited to the range of $10\text{m} \cdot s^{-1} \le v_x \le 33.3\text{m} \cdot s^{-1}$. The lateral tracking performance is constrained by $-\varrho(t) \le e_y \le \varrho(t)$, where $\varrho(t) = 0.2e^{-2t} + 0.05$. To maintain vehicle stability, the difference between the yaw rate and the yaw rate reference must satisfy the stability index k, defined as $\left|\dot{\psi} - \dot{\psi}_d\right| \le k\left|\dot{\psi}_d\right|$, where k is between 0 and 0.165, and $\dot{\psi}_d$ should satisfy the lateral constraint $\left|\dot{\psi}_d\right| \le \mu g / v_x$, as reported in [15]. Thus $\left|\dot{\psi} - \dot{\psi}_d\right| \le 0.165\mu g / v_x$. The yaw rate limitation in the tolerance is therefore defined as $\max\{\dot{\psi}_d(t) - 0.165\,\mu g / v_x, -\mu g / v_x\} \le \dot{\psi}(t) \le \min\{\dot{\psi}_d(t) + 0.165\,\mu g / v_x, \mu g / v_x\}$. The parameters of the proposed controller are chosen as K_{1y} = 0.2, K_{2y} = 5, K_{3y} = 50, K_{4y} = 100, K_{1s} = diag(10, 2.5), K_{2s} = diag (50, 50), $\varpi_{1y} = \varpi_{2y} = \varpi_{3y}$ = 500, $\tau_{1y} = \tau_{2y} = \tau_{3y}$ = 0.9, ϖ_{1s} = diag(500, 500), τ_{1s} = diag(0.9, 0.9), γ_y = 0.5, Υ_s = diag(0.01, 0.01).

5.2. Result and Discussion

The vehicle starts with an initial speed of 22.3 $\text{m} \cdot s^{-1}$ and an initial lateral offset error of 0.15 m on the dry road (μ = 0.9). The vehicle then accelerates to 25.8 $\text{m} \cdot s^{-1}$ by increasing its speed by 1 $\text{m} \cdot s^{-1}$ while making a lane change to the left lane. After that, the vehicle decelerates to 18.5 $\text{m} \cdot s^{-1}$ by decreasing its speed by 2 $\text{m} \cdot s^{-1}$ during another right lane change.

The reference trajectory for the lane change maneuver is designed via five-degree polynomial function:

$$y(t) = a_5 t^5 + a_4 t^4 + a_3 t^3 + a_2 t^2 + a_1 t + a_0$$

with the initial condition: $y_{t=t_o} = y_o$, $\dot{y}_{t=t_o} = 0, \ddot{y}_{t=t_o} = 0$, and the terminal condition: $y_{t=t_f} = y_f$,

$\dot{y}_{t=t_f} = 0, \ddot{y}_{t=t_f} = 0$. The length of the lane change maneuver is 2.5 seconds with $y_o = 0$, and $y_f = 3.75$ for standard lane width. Then, the desired yaw rate is determined by $\dot{\psi}_d = \rho V_x$ where ρ is the curvature of the desired trajectory.

Fig. 2 shows the lateral tracking error of the vehicle. From the result, one can see that the proposed method can guarantee the tracking error always evolve within the performance boundary and converge to zeros at the end. Meanwhile, the SMC control scheme generates larger errors that go beyond the boundary and exhibits a slower convergence rate.

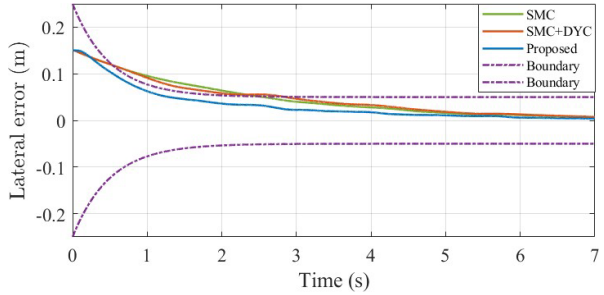

Fig. 2. Lateral error

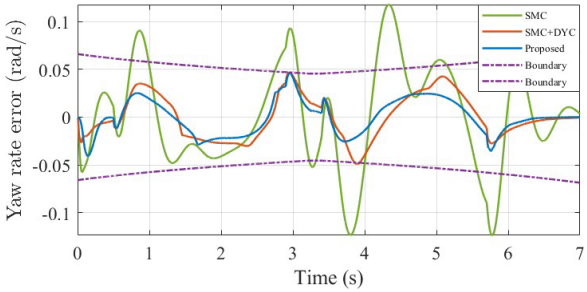

Fig. 3. Yaw rate error

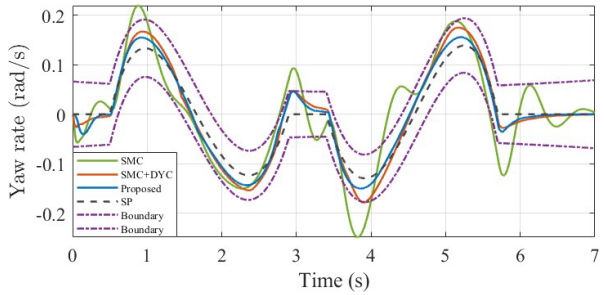

Fig. 4. Yaw rate

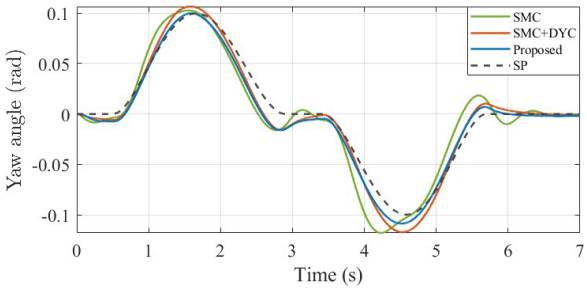

Fig. 5. Yaw angle

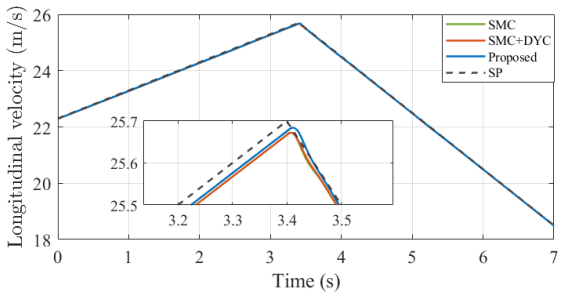

Fig. 6. Longitudinal velocity

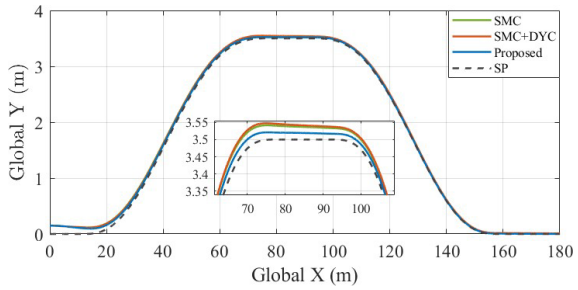

Fig. 7. Global position

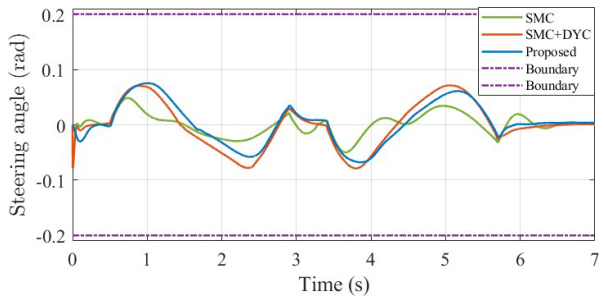

Fig. 8. Steering angle

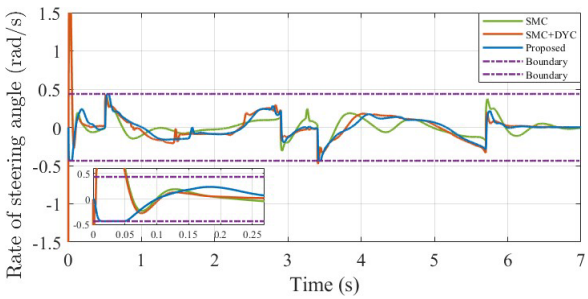

Fig. 9. Rate of steering angle

The comparisons of yaw angle, yaw rate, and yaw rate error are displayed in Fig. 3, 4, and 5 respectively. The results show that with the DYC and the torque allocation algorithm, the vehicle can minimize the deviation of the yaw rate and ensure that the yaw rate is within the allowable range, thus increasing the stability of the vehicle. In comparison, the absence of the DYC component results in greater fluctuations and errors in the yaw rate and yaw angle, which has a negative impact on the stability of the vehicle. For the speed tracking performance, the results in Fig. 6 indicate that all control schemes allow the vehicle to closely track the desired velocity profile during the maneuver, but the proposed method exhibits a higher level of accuracy. Fig. 7 shows the global trajectory of the vehicle. It can be observed that by using the proposed method, the vehicle can achieve faster and more precise lane change maneuvers. Additionally, the overshoot and tracking error is significantly reduced, demonstrating the effectiveness of the proposed method in enhancing the vehicle's performance. The steering angle and steering rate are shown in Fig. 8 and 9. Since there is an initial lateral offset error, the SMC controller generates a fast and large steering angle to steer the vehicle to the reference trajectory, but it causes a significantly high steering rate, which can damage the actuator. In contrast, the proposed method effectively limits the steering rate within the specified bounds, while simultaneously achieving a higher level of tracking performance. This can result in smoother and more controlled lane changes, which can improve passenger comfort and extend actuator life.

6. Conclusion

In this paper, the integrated longitudinal-lateral and yaw rate dynamics of the vehicle are considered simultaneously in the control design to enhance the vehicle's performance in harsh driving conditions. The new adaptive asymmetric time-varying integral barrier Lyapunov control and dynamic surface control are proposed for AFS, longitudinal control, and DYC controller design, such that the system' states and control input signals are guaranteed to be strictly bounded within allowable ranges, while the lumped disturbances are compensated by the RBFNN to enhance the system robustness. Besides, the optimization-based torque allocation algorithm is introduced to effectively distribute driving/braking torque to each in-wheel motor. The simulation results demonstrate the effectiveness and superiority of the proposed control scheme through both quantitative and qualitative comparisons in various driving scenarios when compared to the SMC method.

References

[1] C. Gkartzonikas and K. Gkritza, What have we learned? A review of stated preference and choice studies on autonomous vehicles, Transportation Research Part C: Emerging Technologies, vol. 98, pp. 323-337, 2019, https://doi.org/10.1016/j.trc.2018.12.003

[2] E. Yurtsever, J. Lambert, A. Carballo, and K. Takeda, A survey of autonomous driving: Common practices and emerging technologies, IEEE access, vol. 8, pp. 58443-58469, 2020, https://doi.org/10.1109/ACCESS.2020.2983149

[3] D. Ao, W. Huang, P. K. Wong, and J. Li, Robust backstepping super-twisting sliding mode control for autonomous vehicle path following, IEEE Access, vol. 9, pp. 123165-123177, 2021, https://doi.org/10.1109/ACCESS.2021.3110435

[4] X. Ji, X. He, C. Lv, Y. Liu, and J. Wu, Adaptive-neural-network-based robust lateral motion control for autonomous vehicle at driving limits, Control Engineering Practice, vol. 76, pp. 41-53, 2018, https://doi.org/10.1016/j.conengprac.2018.04.007

[5] Y. Wang, S. Shi, S. Gao, Y. Xu, P. Wang, Active steering and driving/braking coupled control based on flatness theory and a novel reference calculation method, IEEE Access, vol.7, pp.180661-180670, https://doi.org/10.1109/ACCESS.2019.2959941

[6] N. Tork, A. Amirkhani, and S. B. Shokouhi, An adaptive modified neural lateral-longitudinal control system for path following of autonomous vehicles, Engineering Science and Technology, an International Journal, vol. 24, no. 1, pp. 126-137, 2021, https://doi.org/10.1016/j.jestch.2020.12.004

[7] H. Sazgar, S. Azadi, R. Kazemi, A. K. Khalaji, Integrated longitudinal and lateral guidance of vehicles in critical high speed manoeuvres, Proc. of the Institution of Mechanical Engineers, Part K: Journal of Multi-body Dynamics, vol. 233, no. 4, pp. 994-1013, 2019, https://doi.org/10.1177/1464419319847916

[8] H. Pang, R. Yao, P. Wang, and Z. Xu, Adaptive backstepping robust tracking control for stabilizing lateral dynamics of electric vehicles with uncertain parameters and external disturbances, Control Engineering Practice, vol. 110, p. 104781, 2021, https://doi.org/10.1016/j.conengprac.2021.104781

[9] X. Jin, Z. Yu, G. Yin, and J. Wang, Improving vehicle handling stability based on combined AFS and DYC system via robust Takagi-Sugeno fuzzy control, IEEE Transactions on Intelligent Transportation Systems, vol. 19, no. 8, pp. 2696-2707, 2017, https://doi.org/10.1109/TITS.2017.2754140

[10] J. Liu, L. Gao, J. Zhang, and F. Yan, Super-twisting algorithm second-order sliding mode control for collision avoidance system based on active front steering and direct yaw moment control, Proceedings of the Institution of Mechanical Engineers, Part D: Journal of Automobile Engineering, vol. 235, no. 1, pp. 43-54, 2021, https://doi.org/10.1177/0954407020948298

[11] H. Wang, B. Liu, X. Ping, and Q. An, Path tracking control for autonomous vehicles based on an improved MPC, IEEE Access, vol. 7, pp. 161064-161073, 2019, https://doi.org/10.1109/ACCESS.2019.2944894

[12] H. Wu, Z. Si, and Z. Li, Trajectory tracking control for four-wheel independent drive intelligent vehicle based on model predictive control, IEEE Access, vol. 8, pp. 73071-73081, 2020, https://doi.org/10.1109/ACCESS.2020.2987812

[13] A.-T. Nguyen, B.-M. Nguyen, T. Vo-Duy, and M. C. Ta, Steering vector control for lateral force distribution of electric vehicles, in 2022 IEEE Vehicle Power and Propulsion Conference (VPPC), 2022, pp. 1-6: IEEE, https://doi.org/10.1109/VPPC55846.2022.10003321

[14] K. Akka and F. Khaber, Optimal fuzzy tracking control with obstacles avoidance for a mobile robot based on Takagi-Sugeno fuzzy model, Transactions of the Institute of Measurement and Control, vol. 41, no. 10, pp. 2772-2781, 2019. https://doi.org/10.1177/0142331218811462

[15] L. Zhai, T. Sun, and J. Wang, Electronic stability control based on motor driving and braking torque distribution for a four in-wheel motor drive electric vehicle, IEEE Transactions on Vehicular Technology, vol. 65, no. 6, pp. 4726-4739, 2016. https://doi.org/10.1109/TVT.2016.2526663